Accelerated Boundary Element Method for Diffuse Optical Imaging

Josias Elisee, Marc Bonnet, Simon Arridge

▶ **To cite this version:**

Josias Elisee, Marc Bonnet, Simon Arridge. Accelerated Boundary Element Method for Diffuse Optical Imaging. Optics Letters, 2011, 36, pp.4101-4103. 10.1364/OL.36.004101 . hal-00624462

HAL Id: hal-00624462
https://hal.science/hal-00624462v1

Submitted on 17 Sep 2011

HAL is a multi-disciplinary open access archive for the deposit and dissemination of scientific research documents, whether they are published or not. The documents may come from teaching and research institutions in France or abroad, or from public or private research centers.

L'archive ouverte pluridisciplinaire **HAL**, est destinée au dépôt et à la diffusion de documents scientifiques de niveau recherche, publiés ou non, émanant des établissements d'enseignement et de recherche français ou étrangers, des laboratoires publics ou privés.

An Accelerated Boundary Element Method for Diffuse Optical Imaging

Josias Elisee,[1,*] Marc Bonnet,[2] and Simon Arridge[1]

[1] *Centre for Medical Image Computing, University College London, Gower Street, London WC1E 6BT, UK*
[2] *POems (UMR 7231 CNRS-ENSTA-INRIA), Applied Mathematics Department, ENSTA, Paris, France*
[*] *Corresponding author: j.elisee@cs.ucl.ac.uk*

Compiled September 17, 2011

The boundary element method (BEM) is a useful tool in Diffuse Optical Imaging (DOI) when modelling large optical regions whose parameters are piecewise constant, but is computationally expensive. We present here an acceleration technique, the single-level Fast Multipole Method, for a highly lossy medium. The enhanced practicability of the BEM in DOI is demonstrated through test examples on single-layer problems, where order of magnitude reduction factors on solution time are achieved, and on a realistic three-layer model of the neonatal head. Our experimental results agree very closely with theoretical predictions of computational complexity. © 2011 Optical Society of America

OCIS codes: 000.3860, 000.4430, 110.0113

Numerical methods for calculating forward models of light propagation in tissue are extensively used in Diffuse Optical Imaging (DOI). These include the Finite Element Method (FEM) [1] and Finite Volume Method (FVM) [2], which describe the domain in terms of a volume mesh with locally varying absorption coefficient $\mu_{\rm a}$, reduced scattering coefficent $\mu'_{\rm s}$ and refractive index n. Methods based on discretisation only of the boundaries may be prefereable if the domain of interest can be described in terms of closed regions with constant parameters, including the Kirchhoff Approximation [3] and the Boundary Element Method (BEM) [4,5].

BEM applied to DOI is based on boundary integral equations linking density ϕ and current q of the form

$$\int_{\partial\Omega} \partial_\nu G(\boldsymbol{r},\boldsymbol{r}')\phi(\boldsymbol{r}')\,\mathrm{d}S(\boldsymbol{r}') - \frac{1}{D}\int_{\partial\Omega} G(\boldsymbol{r}'-\boldsymbol{r})q(\boldsymbol{r}')\,\mathrm{d}S(\boldsymbol{r}') + \alpha(\boldsymbol{r})\phi(\boldsymbol{r}) = \int_\Omega Q(\boldsymbol{r}')G(\boldsymbol{r}'-\boldsymbol{r})\,\mathrm{d}V(\boldsymbol{r}') \quad (1)$$

where the region $\Omega \subset \mathbb{R}^3$ has uniform optical properties, α is a known geometric factor, $Q(\boldsymbol{r}')$ is a known source and $G(\boldsymbol{R})$, the full-space fundamental solution to the governing equation of DOI, satisfies $(D\Delta+\kappa^2)G+\delta=0$ and is given, in 3D, by

$$G(\boldsymbol{R}) = \exp(-\iota\kappa R)/(4\pi R) \quad (\text{with } R = \|\boldsymbol{R}\|), \quad (2)$$

while $\partial_\nu G(\boldsymbol{r},\boldsymbol{r}') := \boldsymbol{\nu}(\boldsymbol{r}')\cdot\boldsymbol{\nabla}G(\boldsymbol{r}'-\boldsymbol{r})$ is the normal derivative of G. The wavenumber $\kappa = \kappa_{\rm R} + \iota\kappa_{\rm I}$ and the constant D are defined in terms of μ_a and μ_s, the absorption and scattering coefficients of the medium, by

$$\kappa^2 + D^{-1}[\mu_{\rm a} + \iota\omega/c] = 0, \quad D = [3(\mu_{\rm a}+\mu'_{\rm s})]^{-1}$$

with the square root chosen such that $\kappa_{\rm I} < 0$. For multilayer models (1) is written for each layer, a boundary condition of the form $\phi + \ell q = J^-$ (with J^- denoting an incoming flux) is prescribed on the external surface, and the values of ϕ, q on interfaces relative to each adjacent layer are linked by transmission conditions. The BEM [4,5] then consists in discretizing all relevant surfaces into boundary elements and approximating ϕ, q on each element using simple shape functions, resulting in a system of linear equations of the form

$$\mathbb{A}\phi - \mathbb{B}q - \mathbb{Q} = 0 \quad (3)$$

After accounting for all boundary and transmission conditions in (3), a matrix equation on the N remaining, complex-valued, boundary unknowns is obtained.

One of the difficulties in using BEM for problems with large numbers of unknowns, such as medical imaging, is that the matrices involved are fully-populated, leading to excessive computational requirements in memory, and, by implication, solve time. However, recent acceleration strategies such as the Fast Multipole Method (FMM) [6–9] avoid storing dense matrices, and instead make use of matrix-vector products within iterative solvers for the system (3). Although the FMM has been applied to a variety of problems, its application to the complex-valued model used in DOI requires some special considerations, which are described in this paper.

The FMM stems from fast summation methods initially proposed in [9] and implemented in 3D in [10], based on multipole expansions of the relevant Green's function $G(\boldsymbol{r}-\boldsymbol{r}')$ which achieves a separation of the variables $\boldsymbol{r}$ and $\boldsymbol{r}'$. For this purpose, the relative position vector $\boldsymbol{R} = \boldsymbol{r}'-\boldsymbol{r}$ is decomposed into $\boldsymbol{R} = \tilde{\boldsymbol{r}}' + \boldsymbol{R}_0 - \tilde{\boldsymbol{r}}$, with $\boldsymbol{R}_0 = \boldsymbol{r}'_0 - \boldsymbol{r}_0$, $\tilde{\boldsymbol{r}} = \boldsymbol{r}-\boldsymbol{r}_0$ and $\tilde{\boldsymbol{r}}' = \boldsymbol{r}'-\boldsymbol{r}'_0$ in terms of two poles $\boldsymbol{r}_0, \boldsymbol{r}'_0$. With these notations, $G(\boldsymbol{r}'-\boldsymbol{r})$ admits the decomposition [7,11]

$$G(\boldsymbol{r}'-\boldsymbol{r}) \approx \frac{1}{4\pi}\sum_{p=1}^{P} w_p \exp(-\iota\kappa\boldsymbol{s}_p\cdot\tilde{\boldsymbol{r}}')T_p\exp(\iota\kappa\boldsymbol{s}_p\cdot\tilde{\boldsymbol{r}}) \quad (4)$$

in the so-called *diagonal form*, established as a consequence of the Gegenbauer addition theorem [8,12], where the *transfer function* $T_p = T(\boldsymbol{R}_0, \boldsymbol{s}_p)$ is given by

$$T_p = \frac{1}{4\pi}\sum_{\ell=0}^{L}\kappa(-\iota)^{\ell+1}(2\ell+1)h_\ell^{(2)}(\kappa R_0)P_\ell(\hat{\boldsymbol{R}}_0\cdot\boldsymbol{s}_p) \quad (5)$$

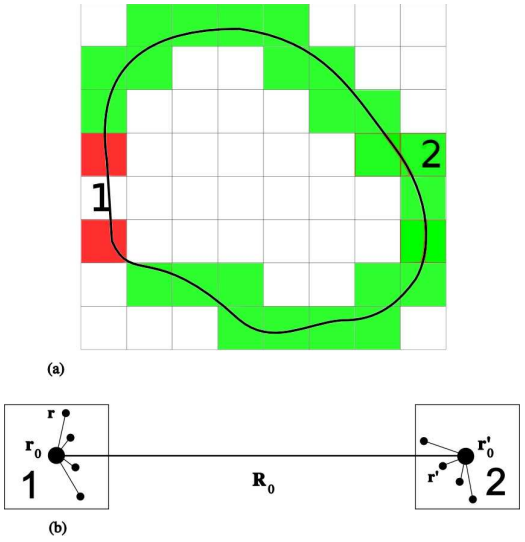

Figure 1. *Single-level FMM for a 2D domain. (a) Interactions close to cell 1 marked in red, far marked in green (e.g. cell 2); (b) matrix-vector multiplication scheme between cell 1 centred at r_0 and cell 2 centred at r'_0*

with $R_0 = \|\boldsymbol{R}_0\|$ and $\hat{\boldsymbol{R}}_0 = \boldsymbol{R}_0/R_0$, and $h_\ell^{(2)}$ and P_ℓ are spherical Hankel functions of second kind and Legendre polynomials, respectively [12]. Decomposition (4) is approximate in that i) an integration over the unit sphere S_2 is replaced with a P-point numerical quadrature (with points $\boldsymbol{s}_p \in S_2$ and weights w_p), and ii) the infinite series defining the exact transfer function $T(\boldsymbol{R}_0, \boldsymbol{s}_p)$ is truncated at level L in (5); however, (4) holds within known error bounds on L and P if [11]

$$\|\boldsymbol{R} - \boldsymbol{R}_0\|/\|\boldsymbol{R}_0\| \leq 2/\sqrt{5} \tag{6}$$

Decomposition of $\partial_\nu G$ is obtained in a similar way by multiplying each summand of (4) by $-\imath\kappa \boldsymbol{s}_p \cdot \boldsymbol{\nu}(\tilde{\boldsymbol{r}}')$.

The separation of the variables $\boldsymbol{r}'$ and $\boldsymbol{r}$ achieved by (4) allows to re-use integrations w.r.t. $\boldsymbol{r}'$ in (1) when changing the collocation point $\boldsymbol{r}$; this is the main acceleration mechanism behind the FMM. Decomposition (4) can be applied recursively, but in this first report, only the single-level FMM is considered. The latter exploits a division of the spatial region containing $\partial\Omega$ into M cubic cells $\mathcal{C}_m$ $(m = 1 \ldots M)$ of equal size (Fig. 1). Integrals in (1) may be evaluated using (4) instead of (2) whenever $\boldsymbol{r}'$ and $\boldsymbol{r}$ belong to two non-adjacent cells $\mathcal{C}_m$ and $\mathcal{C}_{m'}$. The theoretical computational complexity per GMRES iteration of the single-level FMM for Helmholtz-type equations is $O(N^{3/2})$ [7], instead of $O(N^2)$ for the standard BEM.

We summarise our algorithm (following [7, 8, 11]) as

1. Choose spatial grid edge length size a, and assign elements $\{\tau_j\}$ to cells according to their midpoint
2. Build sparse matrices $\mathbb{A}^0, \mathbb{B}^0$ using (2) only for elements and collocation points lying in the same or adjacent cells.
3. For each element $\tau_{n'}$ assigned to cell $\mathcal{C}_{m'}$, compute excitation vectors $\mathbb{V}^A_{m'}, \mathbb{V}^B_{m'}$ with entries:

$$V^A_{m'n'}(\boldsymbol{s}_p) = -\imath\kappa \int_{\tau_{n'}} \exp(-\imath\kappa \boldsymbol{s}_p \cdot \tilde{\boldsymbol{r}}')\, \boldsymbol{s}_p \cdot \boldsymbol{\nu}(\boldsymbol{r}')\, \mathrm{d}S(\tilde{\boldsymbol{r}}')$$
$$V^B_{m'n'}(\boldsymbol{s}_p) = \frac{1}{D} \int_{\tau_{n'}} \exp(-\imath\kappa \boldsymbol{s}_p \cdot \tilde{\boldsymbol{r}}')\, \mathrm{d}S(\tilde{\boldsymbol{r}}') \tag{7}$$

4. For each collocation point $\boldsymbol{r}_n$ assigned to cell $\mathcal{C}_m$, compute excitation vectors $\mathbb{C}_m$, with entries:

$$C_{mn}(\boldsymbol{s}_p) = \exp(\imath\kappa \boldsymbol{s}_p \cdot \tilde{\boldsymbol{r}}_n)\ . \tag{8}$$

5. For each quadrature point $\boldsymbol{s}_p$, for each pair of cells $\mathcal{C}_m$ and $\mathcal{C}'_m$, compute the transfer matrices $\mathbb{T}(\boldsymbol{s}_p)$, with entries $T_{mm'}(\boldsymbol{s}_p)$ given by (5).
6. Apply GMRES iterative solver, with each GMRES iteration requiring matrix-vector products $\mathbb{A}\phi - \mathbb{B}q$

   (a) For each cell $\mathcal{C}_{m'}$, compute the far field $S_{m'}(\boldsymbol{s}_p)$

$$S_{m'}(\boldsymbol{s}_p) = \mathbb{V}^A_{m'}(\boldsymbol{s}_p)\phi_{m'} - \mathbb{V}^B_{m'}(\boldsymbol{s}_p) q_{m'} \tag{9}$$

   (b) Compute the Fourier components of the field in each cell $\mathcal{C}_m$ (with summation running over cells $\mathcal{C}'_m$ that are not adjacent to $\mathcal{C}_m$)

$$G_m(\boldsymbol{s}_p) = \textstyle\sum_{m'} T_{mm'}(\boldsymbol{s}_p) S_{m'}(\boldsymbol{s}_p) \tag{10}$$

   (c) Compute the matrix-vector product:

$$(\mathbb{A}\phi - \mathbb{B}q) = (\mathbb{A}^0\phi - \mathbb{B}^0 q) + \sum_{m=1}^{M} \sum_{p=1}^{P} G_m(\boldsymbol{s}_p) \mathbb{C}_m(\boldsymbol{s}_p) \tag{11}$$

In our implementation, $(\boldsymbol{s}_p, w_p)$ are taken as the Lebedev quadrature points and weights, specifically designed to integrate functions on the unit sphere [13]. For the integrals in (7), which do not involve any singularities, simple Gaussian quadrature was used.

The Diffusion Approximation used in DOI is such that $|\kappa_{\mathrm{I}}| > \kappa_{\mathrm{R}}$. This requires increasing the truncation level L in (4), which in turn affects other computational parameters such as N. Published work on the FMM with $\kappa_{\mathrm{I}} \neq 0$ is scarce. The particular case of a lossy space has been studied in [8] in a half-space and for small $|\kappa_{\mathrm{I}}|/\kappa_{\mathrm{R}}$ (maximum 0.32) only, while a typical value for DOI is $|\kappa_{\mathrm{I}}|/\kappa_{\mathrm{R}} = 9.7$. However, due to the exponential decay of $|G|$, low accuracy in (4) for large distances R is found to affect only marginally the overall solution accuracy, and in the results presented here we used (following [14]) :

$$L = |\kappa a\sqrt{3} + ln(\pi + \kappa a\sqrt{3})| + 6 \tag{12}$$

To assess the efficiency of our implementation, a series of numerical experiments were conducted on homogeneous spheres with increasing radius, and mesh density of 0.65 elements per mm^2, giving the number of

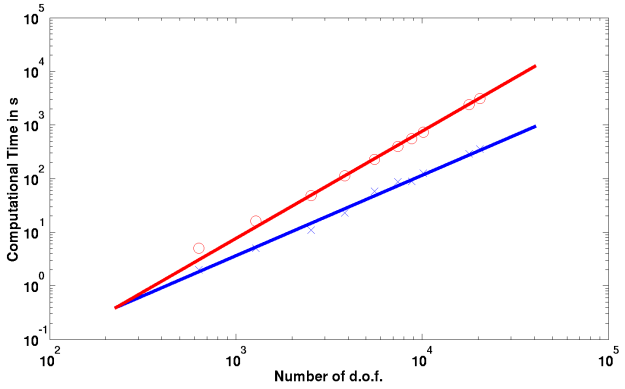

Figure 2. Computation time as a function of number of degrees of freedom for the FMM (blue) and BEM (red).

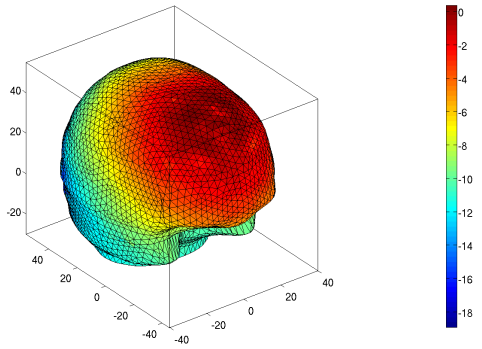

Figure 3. Logarithm of light intensity on cortical surface computed from a 3-layer model

unknowns as $N_T = 634$, 1280, 2536, 3840, 5568, 7424, 8808, 10144, 17920, 20480. Optical parameters were set to $\mu_s' = 1\text{mm}^{-1}$, $\mu_a = 0.01\text{mm}^{-1}$, $n = 1$ and frequency $\omega/2\pi = 100\text{MHz}$. A Gaussian distribution was used as the source term. Both a conventional BEM and the FM-BEM models were solved for each case. The machine used was a 3GHz processor with 32GB of RAM. Figure 2 shows the expected complexity $O(N^2)$ for former and $O(N^{3/2})$ for the latter. The $L2$-errror between the two methods was less than 10^{-3} in all cases.

As an example of direct interest in DOI of the brain, we constructed also a FM-BEM for the multilayer model developed in [4]. We used a high-resolution version of the three-layered neonate's head, with $N = 44356$ [15]. This had about three times as many unknowns as the mesh used in [4] and the resultant dense matrices could not be stored in memory for direct BEM. The FM-BEM solved this problem in 220s, whereas the direct BEM for the reduced problem with 16594 unknowns took 347 seconds. Figure 3 shows the photon density displayed on the inner layer (the cortical surface).

Another application of FM-BEM will be within a coupled BEM-FEM approach [16], where the sparse FEM terms can be explicitly stored and used as an extra term in the matrix-vector calculation (11). In this implementation we considered the collocation BEM framework, which is reflected in the simpler expression for $\mathbb{C}$ in contrast to that for $\mathbb{V}$. However, a Galerkin-BEM implementation is also possible, and may improve performance due to the symmetry properties of the resulting matrices, as well as a simplification of the BEM-FEM coupling.

Development of an efficient FM-BEM code opens the potential to use high resolution anatomical models within DOI, such as in *Diffuse Optical Cortical Mapping* (DOCM) [17]. Such models are readily available for example from high resolution MRI using appriopriate analysis and segmentation tools. However, single-level FMM becomes sub-optimal for model sizes $N = O(5\,10^4)$ and beyond, so implementation of a full multilevel FMM will be required. Finally we note that FMM can be accelerated efficiently using Graphics Processing Units [18], where the difference between FM and conventional BEM is even greater. These extensions will be reported in subsequent publications.

References

1. S. R. Arridge, M. Schweiger, M. Hiraoka and D. T. Delpy Med. Phys., **20**, 299 (1993).
2. V.Y. Soloviev Med. Phys., **33**, 4176, (2006).
3. J. Ripoll, V. Ntziachristos, R. Carminati, and M. Nieto-Vesperinas, Phys. Rev. E **64**, 051917 (2001).
4. J. Sikora, A. Zacharopoulos, A. Douiri, M. Schweiger, L. Horesh, S. Arridge, and J. Ripoll, Physics in Medicine and Biology **51**, 497 (2006).
5. A. D. Zacharopoulos, S. R. Arridge, O. Dorn, V. Kolehmainen, and J. Sikora, Inverse Problems **22**, 1509 (2006).
6. S. Chaillat, M. Bonnet, and J. F. Semblat, Geophys. J. Int. **177**, 509 (2009).
7. R. Coifman, V. Rokhlin, and S. Wandzura, IEEE Antennas Propagat. Mag. **35**, 7 (1993).
8. N. Geng, A. Sullivan, and L. Carin, IEEE Trans. Antennas Propagat. **49**, 740 (2001).
9. L. Greengard and V. Rokhlin, J. Comput. Phys. **73**, 325 (1987).
10. K. E. Schmidt and M. A. Lee, Journal of Statistical Physics **63**, 1223 (1991).
11. E. Darve, J. Comput. Phys. **160**, 195 (2000).
12. M. Abramovitz and I. A. Stegun, Dover, 1970.
13. V. I. Lebedev and D. N. Laikov, Doklady Mathematics **59**, 477 (1999).
14. E. Darve, SIAM J. Numer. Anal. **38**, pp. 98 (2001).
15. A. Tizzard, L. Horesh, R. J. Yerworth, D. S. Holder, and R. H. Bayford, Physiol. Measur. **26**, S251 (2005).
16. J. Elisee, A. Gibson, and S. Arridge, IEEE Trans. Biomed. Eng. **57**, 2737 (2010).
17. J. Elisee, A. Gibson, and S. Arridge, Biomedical Optics Express **2**, 568 (2011).
18. N.A. Gumerov, R. Duraiswami, J. Comput. Phys. **227**, 8290–8313 (2008).